Geospace Concussion: Global reversal of ionospheric vertical plasma drift in response to a sudden commencement

Xueling Shi[1,2], Dong Lin[2], Wenbin Wang[2], Joseph B. H. Baker[1], James M. Weygand[3], Michael D. Hartinger[4], Viacheslav G. Merkin[5], J. Michael Ruohoniemi[1], Kevin Pham[2], Haonan Wu[6], Vassilis Angelopoulos[3], Kathryn A. McWilliams[7], Nozomu Nishitani[8], and Simon G. Shepherd[9]

[1]Department of Electrical and Computer Engineering, Virginia Tech, Blacksburg, VA, USA.
[2]High Altitude Observatory, National Center for Atmospheric Research, Boulder, CO, USA.
[3]Department of Earth, Planetary and Space Sciences, University of California Los Angeles, CA, USA
[4]Space Science Institute, Boulder, CO, USA.
[5]Applied Physics Laboratory, Johns Hopkins University, Laurel, MD, USA
[6]Department of Physics and Astronomy, Clemson University, Clemson, SC, USA
[7]Institute of Space and Atmospheric Studies, University of Saskatchewan, Saskatoon, SK, Canada
[8]Institute for Space-Earth Environmental Research, Nagoya University, Nagoya, Japan
[9]Thayer School of Engineering, Dartmouth College, Hanover, NH, USA

Key Points:

- Dayside ionospheric plasma undergoes a transient motion from downward to upward during a sudden commencement (SC)
- Both observations and simulations show that the reversed vertical drift is a global response of the ionosphere to the SC
- The transient response is caused by a reversal of induced zonal electric field during the SC

Corresponding author: Dong Lin, ldong@ucar.edu

Corresponding author: Xueling Shi, xueling7@vt.edu

Abstract

An interplanetary shock can abruptly compress the magnetosphere, excite magnetospheric waves and field-aligned currents, and cause a ground magnetic response known as a sudden commencement (SC). However, the transient ($<\sim$ 1 min) response of the ionosphere-thermosphere system during an SC has been little studied due to limited temporal resolution in previous investigations. Here, we report observations of a global reversal of ionospheric vertical plasma motion during an SC on 24 October 2011 using $\sim$ 6 s resolution SuperDARN ground scatter data. The dayside ionosphere suddenly moved downward during the magnetospheric compression due to the SC, lasting for only $\sim$ 1 min before moving upward. By contrast, the post-midnight ionosphere briefly moved upward then moved downward during the SC. Simulations with a coupled geospace model suggest that the reversed $\vec{E}\times\vec{B}$ vertical drift is caused by a global reversal of ionospheric zonal electric field induced by magnetospheric compression during the SC.

Plain Language Summary

It is well-known that a shock wave can suddenly compress objects they directly interact with. In this study, we report a special case in the geospace environment in which an interplanetary shock produced a concussion-like response in the ionosphere that was tens of thousands of kilometers away from the location where the shock first impacted. The ionized part of the atmosphere, or the ionosphere, was remotely connected to the magnetosphere - the region of geospace dominated by the Earth's magnetic field - via electric currents. When the magnetosphere was abruptly compressed after the shock arrival, a pair of electric currents flowing along the geomagnetic field lines was generated in the dayside mid-latitudes. The newly generated currents flipped the dayside ionospheric electric field from eastward to westward, leading to a downward motion of dayside ionospheric charged particles. Within one minute, the vertical motion and zonal electric field flipped again to the direction before the compression due to the generation of another pair of electric currents with an opposite sense to the first pair. This study depicts a global picture of the transient ionospheric response using multi-point high-resolution measurements and simulations with a state-of-the-art fully coupled geospace model.

1 Introduction

An interplanetary (IP) shock or a discontinuity in the solar wind can cause a sudden commencement (SC) in ground magnetic perturbations. It is also sometimes called sudden impulse or sudden storm commencement if followed by a geomagnetic storm (Joselyn & Tsurutani, 1990), hereinafter referred to as SC in this paper. Araki (1994) proposed a physical model to characterize the ground magnetic response during an SC. In the magnetosphere, two pairs of field-aligned currents (FACs) with opposite sense and induced electric fields are formed after the compression of the magnetosphere by the IP shock. The FACs and associated ionospheric currents produce a two-pulse signature in ground magnetic perturbations - a preliminary impulse (PI) followed by a main impulse (MI). The enhanced magnetopause current after the impinging of an IP shock produces a stepwise increase in the magnetic horizontal component, known as the SC.

SC impacts on the coupled magnetosphere-ionosphere-thermosphere (M-I-T) system have been extensively studied, including but not limited to the prompt acceleration of radiation belt electrons by the induced electric fields and subsequent ultra-low frequency (ULF) waves, enhanced ionospheric electron/ion temperature, F-region plasma uplift and frictional heating, and the generation of geomagnetically induced currents (e.g., Zong et al., 2009; Hudson et al., 2017; Zou et al., 2017; Belakhovsky et al., 2017; Kappenman, 2003). Global dayside ionosphere uplifting has long been reported to follow the SC due to the enhanced eastward electric fields on the dayside from penetrating interplanetary electric fields (e.g., Mannucci et al., 2005). However, less attention has been paid to the ionospheric downward drift associated with the short-lived westward electric fields preceding the eastward electric fields. Early work since the 1960s reported frequency shifts of high frequency (HF) Doppler sounders associated with SCs, called SCF (e.g., Davies et al., 1962; Kanellakos & Villard, 1962; Huang et al., 1973). A model was proposed by Huang (1976) to explain the HF Doppler effects of SCs and attributed the frequency shifts to the vertical motions of the charged particles in the ionosphere forced by two opposing electric fields. According to HF Doppler sounder observations, SCF(+-) is characterized by a sharp positive frequency deviation spike followed by a prolonged negative frequency deviation, and usually appears in the daytime and evening sectors (06-21 LT) while SCF(-+) is characterized by a negative frequency deviation followed by a positive one, and occurs in the nighttime sector (21-06 LT). Previous reports of the positive preliminary frequency deviations of SCF (i.e., the ionospheric downward motion) found they are mostly constrained to low latitudes and not important due to small amplitudes and a short duration (Kikuchi et al., 1985; Kikuchi, 1986).

To understand the magnetospheric and ionospheric responses to SCs, many numerical studies have also been conducted (e.g., Fujita et al., 2003a, 2003b; Kim et al., 2009; Yu & Ridley, 2011; Zou et al., 2017; Ozturk et al., 2018; Fujita, 2019). However, most previous SC simulations either ignored the processes occurring within one minute after the SC or could not resolve such short time scale due to limited time resolution. For instance, Kim et al. (2009) resolved MI-related vortex with global MHD simulations but could not confirm PI-related vortex with 1-min resolution simulations. Zou et al. (2017) investigated ionospheric SC effects with PFISR observations and global MHD simulations and focused on the upward ion motion and plasma density and temperature variations. The transient impacts of SCs on the I-T system are still not well understood due to lack of self-consistent M-I-T two-way coupled models and observations with high-temporal resolution (< 1 min). In particular, the ionospheric vertical drift related to SCs on global scales and at high temporal resolution (< 1 min) has not yet been well investigated or understood. The main purpose of this study is to investigate the effects of SCs on the I-T system and their temporal evolution using sub-minute, high cadence observations and fully coupled whole geospace modeling.

2 Observations and simulation results

2.1 Data Sets and Models

Space and ground-based data sets and numerical simulations are used to investigate geospace responses to an SC event on 24 October 2011 with a focus on the I-T effects. The data sets include two Time History of Events and Macroscale Interactions during Substorms (THEMIS, Angelopoulos, 2009) spacecraft with THEMIS B located upstream in the solar wind and THEMIS E located inside the magnetosheath just before the SC, the Geostationary Operational Environment Satellite (GOES, Singer et al., 1996) 15 satellite located inside the magnetosphere, and multiple ground magnetometers and Super Dual Auroral Radar Network (SuperDARN) coherent scatter radars (Chisham et al., 2007; Nishitani et al., 2019). The locations of the three spacecraft are shown in Geocentric Solar Ecliptic (GSE) coordinates in Figure 1a. Figure 1b shows the locations of the ionospheric footprint of GOES 15 (red diamond), the Fort Simpson (FSIM) ground magnetometer (blue diamond), and SuperDARN radar fields of view in altitude-adjusted corrected geomagnetic (AACGM) coordinates (Shepherd, 2014).

The Multiscale Atmosphere-Geospace Environment (MAGE) model is a newly developed geospace model that is designed to study mesoscale processes in the coupled geospace system. It consists of the Grid Agnostic MHD for Extended Research Applications (GAMERA) global MHD model of the magnetosphere (B. Zhang et al., 2019; Sorathia et al., 2020), the Rice Convection Model (RCM) model of the ring current (Toffoletto et al., 2003), Thermosphere Ionosphere Electrodynamics General Circulation Model (TIEGCM)

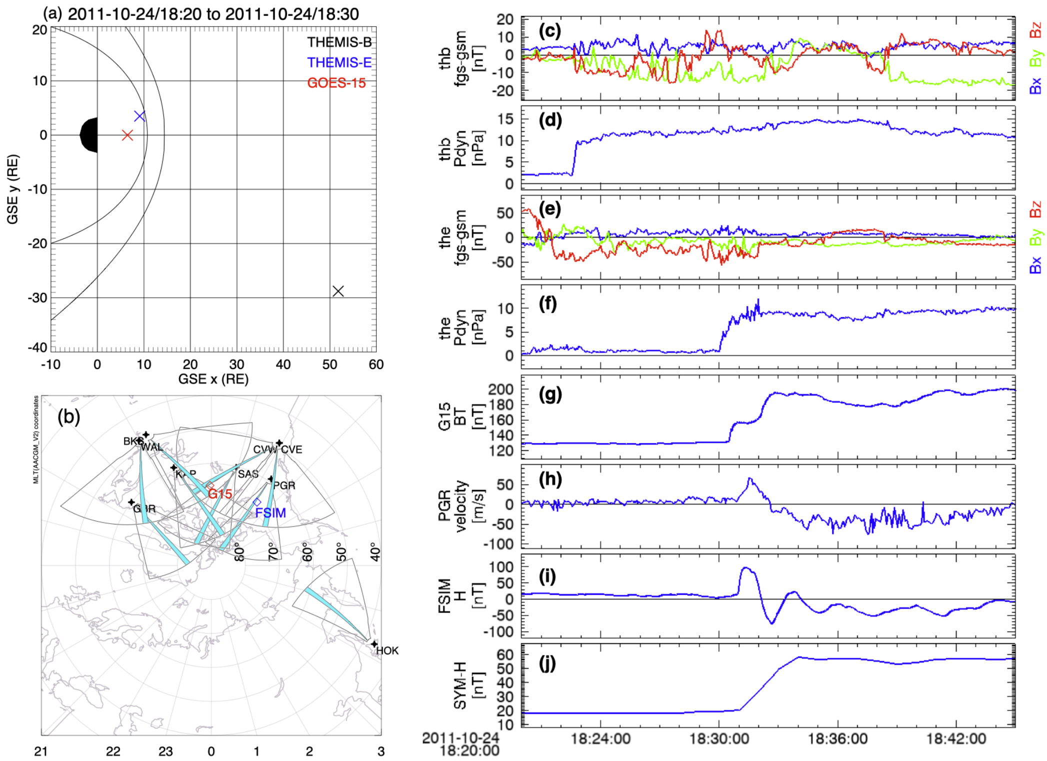

Figure 1. Left: locations of (a) THEMIS B (black) and E (blue) spacecraft and GOES 15 (red) satellite in the X-Y plane in GSE coordinates from 18:20 UT to 18:30 UT on 24 October 2011; (b) locations of the ionospheric footprint of GOES 15 (red), the FSIM ground magnetometer (blue), and SuperDARN radar fields of view and THEMIS mode camping beams (cyan) in AACGM coordinates at 18:32 UT. Right: space and ground observations from 18:20 UT to 18:45 UT of (c-d) interplanetary magnetic field components and solar wind dynamic pressure from THEMIS B spacecraft measurements; (e-f) magnetic field components and dynamic pressure from THEMIS E spacecraft measurements; (g) total magnetic field from the GOES 15 satellite; (h) Doppler velocity measurements from the SuperDARN Prince George radar (beam 12 and gate 11); (i) detrended horizontal magnetic field from the FSIM ground magnetometer; (j) SYM-H index.

of the upper atmosphere (Richmond et al., 1992), and the RE-developed Magnetosphere-Ionosphere Coupler/Solver (REMIX) (Merkin & Lyon, 2010). Details about the model configuration used in this study can be found in Pham et al. (2022) and Lin et al. (2021).

2.2 Observations

Shown in Figure 1(right) are observations during the SC event on 24 October 2011. An IP shock was observed by THEMIS B at 18:22:30 UT with interplanetary magnetic field variations (Figure 1c) and a sharp solar wind dynamic pressure enhancement from about 2 nPa to 10 nPa (Figure 1d). THEMIS E spacecraft, initially inside the magnetosheath, observed gradually enhanced plasma pressure at ∼18:30:00 UT and then crossed the bow shock to enter the solar wind at ∼18:32:00 UT in response to the compression of the magnetosphere by the IP shock. The GOES 15 satellite detected enhanced magnetic field strength at 18:30:30 UT due to the compression by the IP shock (Figure 1g). A transient (∼ 1 min) positive Doppler shift followed by a relatively long lasting negative Doppler shift was observed by multiple SuperDARN radars on the dayside with one example shown in Figure 1h from the Prince George (PGR) radar. A positive PI followed by a negative MI was observed by the FSIM ground magnetometer at 9.7 h magnetic local time (MLT) (Figure 1i), which is consistent with an upward FAC followed by a downward FAC after the SC in the morning sector as described by the Araki model. The SC signature with an enhancement in the SYM-H index (Figure 1j) occurred at 18:31 UT. Note SYM-H only has 1 min resolution. In addition to geomagnetic perturbations, this event was also reported by Shi et al. (2022) and Hartinger et al. (2020) to cause intense geoelectric field perturbations (1.67 V/km at 18:31:41 UT) over Minnesota in the United States.

The Spherical Elementary Current Systems (SECs; Weygand, 2009a, 2009b; Weygand et al., 2011) technique is applied to data from the widely spaced ground magnetometer arrays in North America and Western Greenland to obtain the equivalent ionospheric currents for this SC event. SECs equivalent currents (black vectors) and vertical current density (red-blue color map) are shown in Figure 2 top panels during (a) pre-SC at 18:30:00 UT, (b) PI phase at 18:31:30 UT, and (c) MI phase at 18:33:30 UT. The vertical yellow lines indicate local noon. The SECs equivalent currents from 18:25:00 UT to 18:31:00 UT look similar to those shown in Figure 2a with an anti-clockwise ionospheric current vortex and an upward vertical current (red) in the postnoon sector above 60° geographic latitude and an azimuthally extended downward current (blue) at 65°-70° geographic latitude. The PI related vertical currents first appeared at 18:31:00 UT at lower latitudes and moved poleward with an upward current (red) in the morning and a downward current (blue) in the afternoon sector at 18:31:30 UT as shown in Figure 2b. Figure 2c presents the follow up MI related vertical currents that are opposite to those in the PI phase, but is similar to the pre-SC currents (Figure 2a) with much stronger intensity and well defined current vortexes. These results are consistent with two pairs of FACs with opposite sense generated during the PI and MI phases from the physical model of SC in Araki (1994). An animation showing the evolution of the PI and MI related SECs currents at 10 s cadence can be found in the Supporting Information.

Ground backscatter echoes from SuperDARN coherent scatter radars are used to monitor ionospheric vertical drifts as shown in the bottom panels of Figure 2. Ground scatter echoes are typically formed during the daytime due to the high vertical gradient in the refractive index. The transmitted signal bends toward the ground and is reflected from surface roughness and returns to the radar following the same path. SuperDARN ground backscatter is sensitive to vertical ionospheric motions (Ponomarenko et al., 2003; Menk et al., 2003), and can be used to measure the vertical motion of the ionospheric layers through sunrise and sunset and also the vertical plasma motion associated with traveling ionospheric disturbances (e.g., Milan et al., 2013). In this paper, for the first time, this technique is used to study ionospheric vertical drifts associated with an

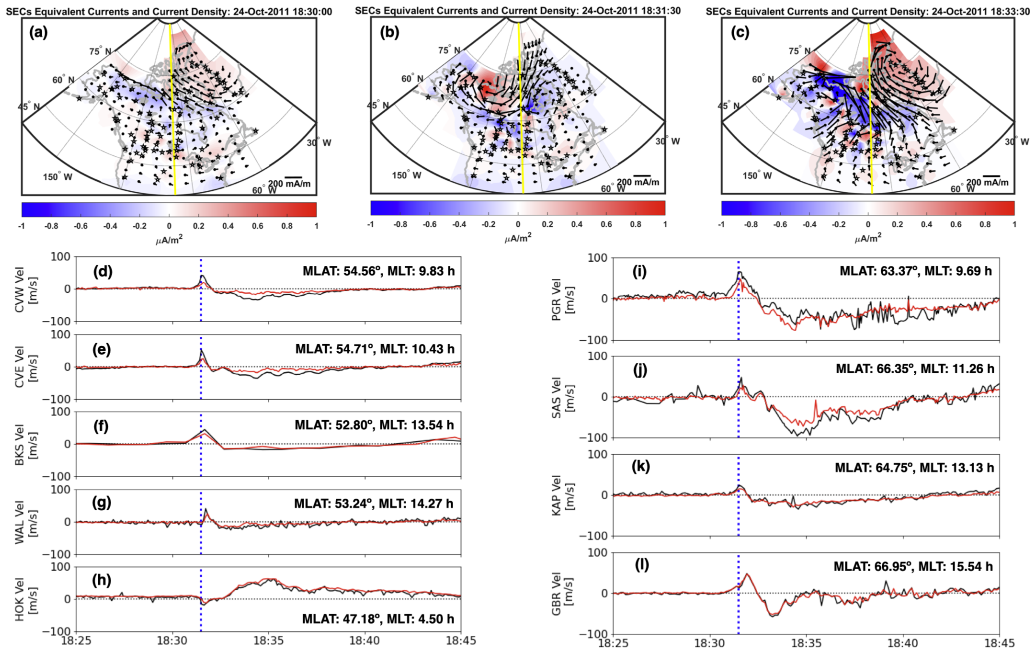

Figure 2. Top: Equivalent ionospheric currents (black vectors) and current density (red-blue color map with amplitude and sign given in the color bar at the bottom) at (a) 18:30:00 UT during pre-SC period, (b) 18:31:30 UT during the PI phase, (c) 18:33:30 UT during the MI phase. The vertical yellow line indicates local noon. Bottom: Doppler velocity from multiple Super-DARN radars (d-h) at middle latitudes and (i-l) high latitudes from 18:25:00 UT to 18:45:00 UT on 24 October 2011.

SC. This is made possible due to radars operating in a mode called THEMIS mode which includes a camping beam; one that is revisited repeatedly during a typical scan. The THEMIS mode is capable of sampling the camping beam (color coded in cyan in Figure 1b) every ~ 6 s and therefore capturing transient variations of < 1 min associated with the SC.

The bottom panels in Figure 2 show Doppler velocity variations in ground scatter from multiple SuperDARN radars at middle to high latitudes. Black traces indicate Doppler velocity obtained from a specific range-gate cell with the largest preliminary impulse observed from the camping beam except for the BKS radar in Figure 2f which shows observations from one normal beam 18 with a temporal resolution of 1 min. The median velocity across multiple range gate cells from the selected beams at each recording time was calculated and shown as red traces. The MLAT/MLT location of the ionospheric reflection point of ground scatter at a specified range-gate cell is calculated assuming an altitude of 250 km (Bristow et al., 1994) and shown on the right of each panel. A transient (1-2 min) positive Doppler shift followed by longer lasting (~ 7 min) negative Doppler shift was observed by multiple SuperDARN radars on the dayside. Blue vertical dotted lines indicate the time at 18:31:30 UT when the PGR radar first observed the peak of the positive impulse. By contrast, observations from the Hokkaido East (HOK) radar located post-midnight at ~ 4.5 h MLT show the opposite Doppler velocity impulses (Figure 2h), that is, a transient negative Doppler shift followed by longer lasting positive one. This is consistent with the HF Doppler sounder observations of SCF (+-) on the dayside and SCF(-+) in the nighttime sector (21-06 LT). The positive (negative) Doppler velocity from SuperDARN ground scatter indicates a downward (upward) plasma motion which might be driven by a westward (eastward) electric field associated with the SC. Note that the BKS radar only shows a clear positive impulse from Beams 18 to 22 (B18 are shown in Figure 2f). Due to a lower temporal resolution (1 min), the positive impulse only consists of 1-2 data points which makes it difficult to be connected with any physical phenomenon without the context provided by other high temporal resolution radar observations.

2.3 MAGE Simulations

In this study, we used the solar wind parameters measured by THEMIS B spacecraft to drive the MAGE model. As shown in Figure 1, THEMIS B was located upstream of the bow shock, which provided closer to real-time information on the IP shock before it arrived at the Earth with higher temporal resolution, compared to OMNI data. The transient reversal of vertical plasma drifts shown in Figure 2 was reproduced by the MAGE model. Figures 3a and 3b show the vertical plasma drift sampled from TIEGCM results at two SuperDARN radar measurement locations, beam 12 of PGR (dayside near 9.7 h MLT) and beam 4 of HOK (nightside at 4.5 h MLT), respectively. In this study, TIEGCM has a time step of 5s and is output every 10 s. The observational data are shown with the magenta and green curves for the two radars and the simulation results are shown in black. Note that the SuperDARN Doppler velocity, which is positive for downward, were transformed into the vertical direction by flipping the sign to directly compare with TIEGCM outputs in Figures 3a-3b. The vertical drifts sampled at PGR turned downward at 18:31 UT during the SC with a maximum speed of ~ 50 m/s and became positive (upward) after 18:32 UT. The sampled vertical drifts at HOK showed a transient upward motion of ~ 20 m/s during the SC before turning downward after the SC. Note that for this plot the SuperDARN measurements were shifted back in time by 30 s in order to match the maximum downward drifts simulated by the model. The deviation is likely due to uncertainty in the timing of solar wind parameters used to drive the model.

The similarity in measurements at multiple SuperDARN radars distributed widely in local time and latitude suggests that the vertical plasma drift reversal is a global effect. Figures 3c and 3d show the keograms of vertical plasma drift sampled by the PGR (9.7 h MLT) and HOK (4.5 h MLT) radars, respectively. The prenoon vertical drift was

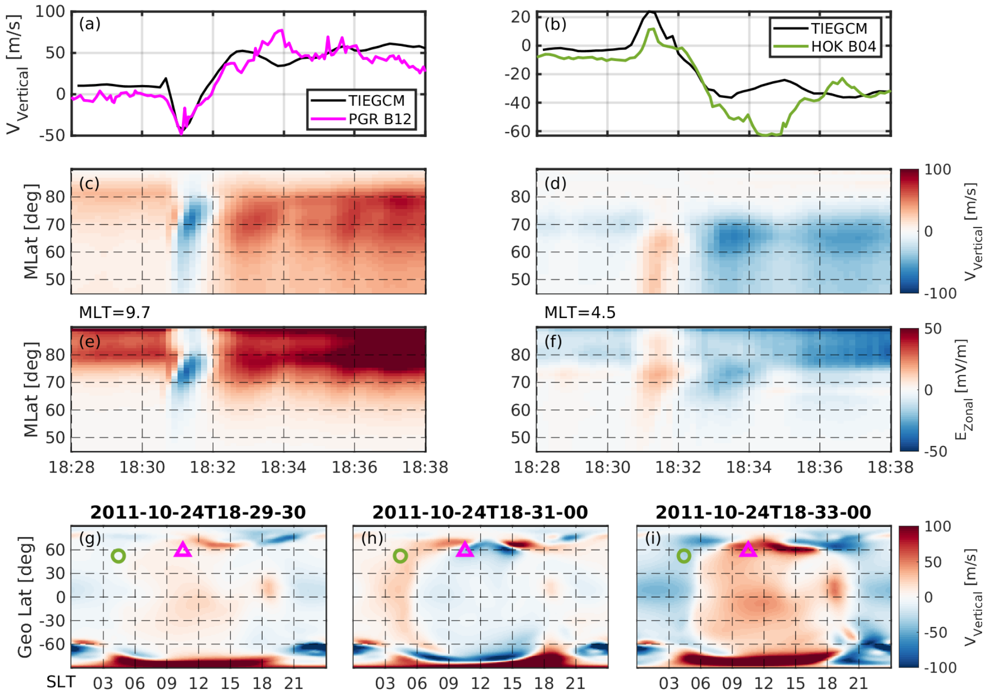

Figure 3. (a-b) Median vertical plasma drifts measured by the SuperDARN PGR radar (magenta) and HOK radar (green), and TIEGCM samplings at the same locations (black). (c-f) Keograms of vertical plasma drifts and zonal electric field at 9.7 h MLT and 4.5 h MLT. (g-i) Vertical plasma drifts sampled at a mean altitude of 255 km from TIEGCM. The magenta triangle and green circle stand for the locations of the PGR and HOK radar observations, respectively.

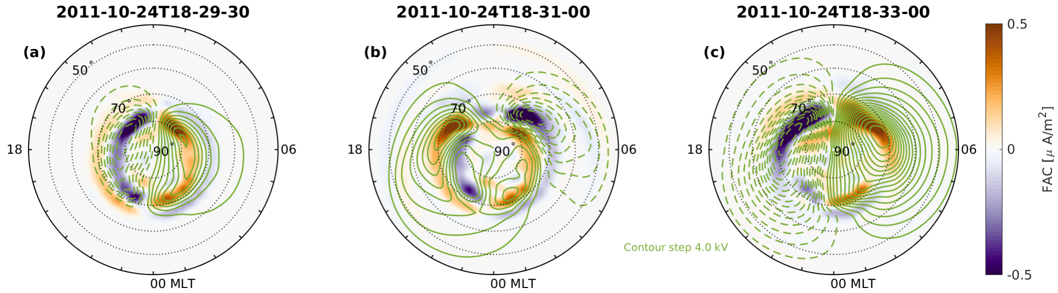

Figure 4. MAGE-simulated northern ionospheric FACs (purple-orange color map) and convection responses to the IP shock. Positive currents (orange) are downward. The green contours show the convection potential separated by every 4.0 kV. Solid curves show positive potential.

downward over a broad range of latitudes for about one minute from 18:30:50 UT to 18:31:50 UT during the PI phase, while before and after the PI, it was upward at all latitudes. By contrast, in the post-midnight sector, the vertical drift was downward at high latitudes but it reversed to upward at middle and low latitude during the PI phase. This ionospheric plasma motion is well described by the $\vec{E}\times\vec{B}$ drift. Figures 3e and 3f show the keograms of zonal electric fields at the same two MLTs. During the PI phase, the zonal electric field was westward in the prenoon sector and eastward in the post-midnight sector, which is consistent with the vertical drift response.

In Figures 3(g-i), we use the simulation results to depict the global picture of the vertical plasma drift (zonal electric field) response during the SC. The vertical drifts were sampled from TIEGCM outputs at a mean altitude of 255 km at the same three UTs shown in Figures 2 (a-c) with the 30 s shift taken into account. The locations of PGR and HOK measurements are denoted with a magenta triangle and a green circle, respectively. Before the SC at 18:29:30 UT, the vertical plasma drifts were a few tens of m/s upward on the dayside ($6 < SLT < 18$) and slightly downward on the nightside. During the PI phase at 18:31:00 UT, however, the vertical drifts globally reversed to downward on the dayside and upward on the nightside. The dayside downward plasma drift reached a few tens of m/s at middle and low latitudes but exceeded 100 m/s at auroral latitudes. The globally reversed vertical drifts only lasted for about one minute before they were reversed again, at 18:32:00 UT. The dayside upward drifts after the SC, e.g., at 18:33:00 UT, were much stronger than those before the SC.

To understand the cause of the transient reversal of ionospheric vertical plasma drifts and zonal electric fields, we analyzed the electrodynamic ionospheric response during the SC with MAGE simulation results. Figure 4 shows the northern ionospheric FACs (purple-orange color map) and convection potential (green contour) at the same three times as shown in Figures 3(g-i). Before the shock arrival (Figure 4a), the ionosphere showed a typical pattern of a pair of Region-1 FACs poleward of a pair of Region-2 FACs and two cell convection with the dawnside (duskside) at positive (negative) potentials. As the shock front arrived and propagated across the Earth (Figure 4b), a pair of Region-2 sense FACs was generated at dayside mid-latitudes that propagated poleward. The postnoon downward FAC and prenoon upward FAC requires a westward electric field for current closure, which drives a downward plasma motion on the dayside. The two-cell convection before the SC was overtaken by a reversed two-cell convection gradually moving from dayside to nightside. After the shock front completely passed over the Earth (Figure 4c), the dayside ionospheric electric field reversed to eastward and the convection returned to the regular two-cell pattern. An animation showing the MAGE-simulated evolution of FACs and ionospheric convection pattern from 18:25:00 UT to 18:45:00 UT is provided in the supporting information. The evolution of two pairs of FACs and their poleward propagation from MAGE simulations are consistent with those from the SECs measurements in Figures 2(a-c).

3 Discussion and Summary

Although the geospace response to an IP shock on scales of more than several minutes has been well investigated, the transient vertical ionospheric motion at sub-minute resolution is scrutinized for the first time with high temporal resolution observations and a coupled geospace model, the MAGE simulations. The THEMIS E spacecraft inside the magnetosheath observed the arrival of the IP shock at ∼18:30:00 UT (Figures 1e-1f). After about 30 s, the GOES-15 satellite located near noon detected the compression of the magnetosphere (Figure 1g). On the ground, the PI- and MI-related FACs were clearly seen following the SC as shown in Figures 2b-2c. MAGE simulations reproduced the geospace responses including the westward and then eastward induced electric fields in the dayside magnetosphere-ionosphere, two pairs of FACs with opposite sense, and ionospheric convection reconfiguration associated with the newly formed FACs after the SC as shown in Figure 4. Multiple-point radar measurements and the MAGE simulation results reveal that the concussion is a global response of the ionosphere to the IP shock. Figure 2 shows that transient downward motion was detected by all SuperDARN radars on the dayside, while the HOK radar on the nightside detected upward ionosphere motion. Although this study focuses on SuperDARN measurements, the transient vertical ionospheric motion was also detected by other facilities. As shown in Figure S1, the Communications/Navigation Outage Forecasting System (CNOFS) satellite (de La Beaujardière et al., 2004) detected a transient downward ion drift velocity of up to 30 m/s from 18:31:00 UT to 18:32:12 UT at 6.6 h MLT near the magnetic equator, similar to those reported by R. Zhang et al. (2022) with a focus on ULF waves during SCs using CNOFS satellite observations at a single location. MAGE simulation results reveal that the vertical plasma drift was globally temporarily reversed on both the dayside and nightside (Figures 3g-3i). The PGR radar observations show the downward motion on the dayside reached ∼70 m/s at high latitudes (Figure 2i).

We suggest that the downward and subsequent upward ionospheric plasma vertical drifts on the dayside were mainly driven by induced electric fields through $\vec{E} \times \vec{B}$ with a transient westward electric field followed by a long-lasting eastward electric field in the dayside magnetosphere and ionosphere. This evolution is identified in the SuperDARN observations and reproduced by the MAGE simulations (Figures 3a and 3b). Alternatively, the positive Doppler velocity in the SuperDARN ground scatter measurements could result from changes in ionospheric refractive index and ray reflection height. For instance, solar flares can instantaneously enhance the ionospheric electron density and lower the F-region reflection height, causing the so-called Doppler flash (e.g., Kikuchi et al., 1986; Chakraborty et al., 2018, 2021). However, this mechanism likely only plays a minor role in the current study. We examined the vertical electron density profiles and time series of F2 peak height (HmF2) at the locations of the PGR and HOK measurements (Figures S2-S3) and found the relative variation of electron density was only 2% and HmF2 variation was only ~ 2 km during the PI phase, inadequate to cause the Doppler shift measured by the radars. Nevertheless, it is possible that in some regions where shock aurora are generated associated with the SC (Liu et al., 2015; Zhou et al., 2017), changes in electron density might play a role. A further examination of the I-T effects during SCs (e.g., shock aurora and electron temperature variations) is deferred to a future study using events when observations of these parameters are available (e.g., incoherent scatter radar measurements from the 17 March 2015 storm).

To summarize, high-temporal resolution observations and the MAGE model simulation are used to investigate the effects of an SC on the geospace system, particularly on the I-T system during the PI phase. We report for the first time using SuperDARN ground scatter observations that the ionosphere undergoes a globally downward motion on the dayside and upward motion in the post midnight sector over 1 min during the PI phase, before it was gradually up lifted by an eastward electric field on the dayside during the longer-lasting MI phase. The high cadence outputs from the coupled geospace model of MAGE reveals for the first time that the ionospheric vertical motion related to SC is a global phenomenon with a larger impact than previously expected. This study advances our understanding of the effects of SCs in several ways:

1. Most previous studies focused on the dayside uplifting of the ionosphere due to limited temporal resolution while this study found that a transient downward drift (< 1 min) precedes the ionosphere uplifting on the dayside following the SC.
2. This study utilized high temporal resolution (~ 6 s) ground scatter signatures in SuperDARN data to estimate ionospheric vertical drifts associated with an SC, whereas other SuperDARN observations using 1 min resolution data focused on ionospheric convection reconfiguration and radar backscatter echo responses associated with SCs (e.g., Coco et al., 2005; Kane & Makarevich, 2010; Boudouridis et al., 2011; Hori et al., 2012). Simultaneous observations from multiple SuperDARN radars provide direct evidence of the existence of the SC-related transient vertical drift in the ionosphere over a larger scale and with larger amplitudes than previously thought (e.g., Kikuchi et al., 1985; Kikuchi, 1986).
3. The coupled geospace model MAGE simulations with high temporal resolution revealed for the first time that the transient ion vertical drift associated with an SC is a global phenomenon (changes seen from the dayside to the nightside, and from the polar region to the equatorial region), whereas most previous MHD simulations concentrated on processes above 1 min time scale.

Acknowledgments
We thank Dr. Gang Lu for an internal review. XS is supported by NASA awards 80NSSC21K1677 and 80NSSC19K0907 and NSF awards AGS-1935110 and AGS-2025570. This work is also supported by NASA GCR grant 80NSSC17K0013, DRIVE Science Center for Geospace Storms (CGS) under grant 80NSSC20K0601, LWS grants 80NSSC20K0356, 80NSSC19K0080, 80NSSC17K0679, 80NSSC21K0008, and 80NSSC20K0199, and NSF CEDAR grant 2033843. JMW was supported by NASA contracts NAS5-02099, 80GSFC17C0018, 80NSSC18K1227, and 80NSSC20K1364. We acknowledge SPEDAS (Angelopoulos et al., 2019) for loading data and generate Figure 1right. The SECs are produced from the AUTUMNX, CARISMA, NRCan, GIMA, DTU Greenland, STEP, THEMIS, MACCS, McMAC, USGS, and Falcon magnetometer arrays. The authors acknowledge the use of SuperDARN data. Funding for operation of the CVW and CVE SuperDARN radars is provided by NSF grant AGS-1934997. This material is based upon work supported by the National Center for Atmospheric Research (NCAR), which is a major facility sponsored by the National Science Foundation under Cooperative Agreement No. 1852977. Computing resources were provided by the High Altitude Observatory at NCAR's Computational and Information Systems Laboratory (CISL).

Data Availability Statement

The SECs are located at `http://vmo.igpp.ucla.edu/data1/SECS/`. The SYM-H index used in this paper was provided by the WDC for Geomagnetism, Kyoto (`http://wdc.kugi.kyoto-u.ac.jp/wdc/Sec3.html`). Access to SuperDARN data can be found at `http://vt.superdarn.org/tiki-index.php?page=Data+Access`. Data from the THMEIS mission can be found at `http://themis.ssl.berkeley.edu/data/themis/`. The GOES magnetic field data can be found at `https://satdat.ngdc.noaa.gov/sem/goes/data/full/`. The MAGE simulation data are saved at this data repository: https://doi.org/10.5065/xj5m-8t12.

References

Angelopoulos, V. (2009). The themis mission. In *The themis mission* (pp. 5–34). Springer. doi: 10.1007/978-0-387-89820-9_2

Angelopoulos, V., Cruce, P., Drozdov, A., Grimes, E., Hatzigeorgiu, N., King, D., ... others (2019). The space physics environment data analysis system (spedas). *Space science reviews*, *215*(1), 1–46.

Araki, T. (1994). A physical model of the geomagnetic sudden commencement. *GEOPHYSICAL MONOGRAPH-AMERICAN GEOPHYSICAL UNION*, *81*, 183–183.

Belakhovsky, V., Pilipenko, V., Sakharov, Y. A., Lorentzen, D., & Samsonov, S. (2017). Geomagnetic and ionospheric response to the interplanetary shock on january 24, 2012. *Earth, Planets and Space*, *69*(1), 1–25.

Boudouridis, A., Lyons, L. R., Zesta, E., Weygand, J. M., Ribeiro, A. J., & Ruohoniemi, J. M. (2011). Statistical study of the effect of solar wind dynamic pressure fronts on the dayside and nightside ionospheric convection. *Journal of Geophysical Research: Space Physics*, *116*(A10). Retrieved from `https://agupubs.onlinelibrary.wiley.com/doi/abs/10.1029/2011JA016582` doi: https://doi.org/10.1029/2011JA016582

Bristow, W. A., Greenwald, R. A., & Samson, J. C. (1994). Identification of high-latitude acoustic gravity wave sources using the goose bay hf radar. *Journal of Geophysical Research: Space Physics*, *99*(A1), 319-331. Retrieved from `https://agupubs.onlinelibrary.wiley.com/doi/abs/10.1029/93JA01470` doi: https://doi.org/10.1029/93JA01470

Chakraborty, S., Qian, L., Ruohoniemi, J. M., Baker, J. B. H., Mclnerney, J. M., & Nishitani, N. (2021). The role of flare-driven ionospheric electron density changes on the doppler flash observed by superdarn hf radars. *Journal of Geophysical Research: Space Physics*, *126*(8), e2021JA029300. Retrieved from `https://agupubs.onlinelibrary.wiley.com/doi/abs/10.1029/2021JA029300` (e2021JA029300 2021JA029300) doi: https://doi.org/10.1029/2021JA029300

Chakraborty, S., Ruohoniemi, J. M., Baker, J. B. H., & Nishitani, N. (2018). Characterization of Short-Wave Fadeout Seen in Daytime SuperDARN Ground Scatter Observations. *Radio Science*, *53*(4), 472–484. Retrieved from `https://agupubs.onlinelibrary.wiley.com/doi/abs/10.1002/2017RS006488` doi: 10.1002/2017RS006488

Chisham, G., Lester, M., Milan, S. E., Freeman, M. P., Bristow, W. A., Grocott, A., ... Walker, A. D. M. (2007, Jan 01). A decade of the Super Dual Auroral Radar Network (SuperDARN): scientific achievements, new techniques and future directions. *Surveys in Geophysics*, *28*(1), 33–109. Retrieved from `https://doi.org/10.1007/s10712-007-9017-8` doi: 10.1007/s10712-007-9017-8

Coco, I., Amata, E., Marcucci, M. F., De Laurentis, M., Villain, J. P., Hanuise, C., & Candidi, M. (2005). Effects on superdarn hf radar echoes of sudden impulses of solar wind dynamic pressure. *Annales Geophysicae*, *23*(5), 1771–1783. Retrieved from `https://angeo.copernicus.org/articles/23/1771/2005/` doi: 10.5194/angeo-23-1771-2005

Davies, K., Watts, J. M., & Zacharisen, D. H. (1962). A study of f 2-layer effects as observed with a doppler technique. *Journal of Geophysical Research (1896-1977)*, *67*(2), 601-609. Retrieved from `https://agupubs.onlinelibrary.wiley.com/doi/abs/10.1029/JZ067i002p00601` doi: https://doi.org/10.1029/JZ067i002p00601

de La Beaujardière, O., et al. (2004). C/nofs: A mission to forecast scintillations. *Journal of Atmospheric and Solar-Terrestrial Physics*, *66*(17), 1573–1591. doi: 10.1016/j.jastp.2004.07.030

Fujita, S. (2019). Response of the magnetosphere–ionosphere system to sudden changes in solar wind dynamic pressure. *Reviews of Modern Plasma Physics*, *3*(1), 1–34.

Fujita, S., Tanaka, T., Kikuchi, T., Fujimoto, K., Hosokawa, K., & Itonaga, M. (2003a). A numerical simulation of the geomagnetic sudden commencement: 1. generation of the field-aligned current associated with the preliminary impulse. *Journal of Geophysical Research: Space Physics*, *108*(A12). Retrieved from `https://agupubs.onlinelibrary.wiley.com/doi/abs/10.1029/2002JA009407` doi: https://doi.org/10.1029/2002JA009407

Fujita, S., Tanaka, T., Kikuchi, T., Fujimoto, K., & Itonaga, M. (2003b). A numerical simulation of the geomagnetic sudden commencement: 2. plasma processes in the main impulse. *Journal of Geophysical Research: Space Physics*, *108*(A12). Retrieved from `https://agupubs.onlinelibrary.wiley.com/doi/abs/10.1029/2002JA009763` doi: https://doi.org/10.1029/2002JA009763

Hartinger, M. D., Shi, X., Lucas, G. M., Murphy, B. S., Kelbert, A., Baker, J. B. H., ... Bedrosian, P. A. (2020). Simultaneous observations of geoelectric and geomagnetic fields produced by magnetospheric ulf waves. *Geophysical Research Letters*, *47*(18), e2020GL089441. Retrieved from `https://agupubs.onlinelibrary.wiley.com/doi/abs/10.1029/2020GL089441` (e2020GL089441 10.1029/2020GL089441) doi: https://doi.org/10.1029/2020GL089441

Hori, T., Shinbori, A., Nishitani, N., Kikuchi, T., Fujita, S., Nagatsuma, T., ... Seki, K. (2012). Evolution of negative si-induced ionospheric flows observed by superdarn king salmon hf radar. *Journal of Geophysical Research: Space Physics*, *117*(A12). Retrieved from `https://agupubs.onlinelibrary.wiley.com/doi/abs/10.1029/2012JA018093` doi: https://doi.org/10.1029/2012JA018093

Huang, Y.-N. (1976). Modeling hf doppler effects of geomagnetic sudden commencements. *Journal of Geophysical Research (1896-1977)*, *81*(1), 175-182. Retrieved from `https://agupubs.onlinelibrary.wiley.com/doi/abs/10.1029/JA081i001p00175` doi: https://doi.org/10.1029/JA081i001p00175

Huang, Y.-N., Najita, K., & Yuen, P. (1973). The ionospheric effects of geomagnetic sudden commencements as measured with an hf doppler sounder at hawaii. *Journal of Atmospheric and Terrestrial Physics*, *35*(1), 173-181. Retrieved from `https://www.sciencedirect.com/science/article/pii/0021916973902250` doi: https://doi.org/10.1016/0021-9169(73)90225-0

Hudson, M., Jaynes, A., Kress, B., Li, Z., Patel, M., Shen, X.-C., ... Wygant, J. (2017). Simulated prompt acceleration of multi-mev electrons by the 17 march 2015 interplanetary shock. *Journal of Geophysical Research: Space Physics*, *122*(10), 10,036-10,046. Retrieved from `https://agupubs.onlinelibrary.wiley.com/doi/abs/10.1002/2017JA024445` doi: https://doi.org/10.1002/2017JA024445

Joselyn, J. A., & Tsurutani, B. T. (1990). Geomagnetic sudden impulses and storm sudden commencements: A note on terminology. *Eos, Transactions American Geophysical Union*, *71*(47), 1808-1809. Retrieved from `https://agupubs.onlinelibrary.wiley.com/doi/abs/10.1029/90EO00350` doi: https://doi.org/10.1029/90EO00350

Kane, T. A., & Makarevich, R. A. (2010). Hf radar observations of the f region ionospheric plasma response to storm sudden commencements. *Journal of Geophysical Research: Space Physics*, *115*(A7). Retrieved from `https://agupubs.onlinelibrary.wiley.com/doi/abs/10.1029/2009JA014974` doi: https://doi.org/10.1029/2009JA014974

Kanellakos, D. P., & Villard, O. G. (1962). Ionospheric disturbances associated with the solar flare of september 28, 1961. *Journal of Geophysical Research (1896-1977)*, *67*(6), 2265-2277. Retrieved from `https://agupubs.onlinelibrary.wiley.com/doi/abs/10.1029/JZ067i006p02265` doi: https://doi.org/10.1029/JZ067i006p02265

Kappenman, J. G. (2003). Storm sudden commencement events and the associated geomagnetically induced current risks to ground-based systems at low-latitude and midlatitude locations. *Space weather*, *1*(3).

Kikuchi, T. (1986). Evidence of transmission of polar electric fields to the low latitude at times of geomagnetic sudden commencements. *Journal of Geophysical Research: Space Physics*, *91*(A3), 3101-3105. Retrieved from `https://agupubs.onlinelibrary.wiley.com/doi/abs/10.1029/JA091iA03p03101` doi: https://doi.org/10.1029/JA091iA03p03101

Kikuchi, T., Ishimine, T., & Sugiuchi, H. (1985). Local time distribution of hf doppler frequency deviations associated with storm sudden commencements. *Journal of Geophysical Research: Space Physics*, *90*(A5), 4389-4393. Retrieved from `https://agupubs.onlinelibrary.wiley.com/doi/abs/10.1029/JA090iA05p04389` doi: https://doi.org/10.1029/JA090iA05p04389

Kikuchi, T., Sugiuchi, H., Ishimine, T., Maeno, H., & Honma, S. (1986). Solar-terrestrial disturbances of June-September 1982, IV. IONOSPHERIC DISTURBANCES 11. HF DOPPLER OBSERVATIONS. *Journal of the Radio Research Laboratories*, *33*(1), 239-255.

Kim, K.-H., Park, K. S., Ogino, T., Lee, D.-H., Sung, S.-K., & Kwak, Y.-S. (2009). Global mhd simulation of the geomagnetic sudden commencement on 21 october 1999. *Journal of Geophysical Research: Space Physics*, *114*(A8). Retrieved from `https://agupubs.onlinelibrary.wiley.com/doi/abs/10.1029/2009JA014109` doi: https://doi.org/10.1029/2009JA014109

Lin, D., Sorathia, K., Wang, W., Merkin, V., Bao, S., Pham, K., . . . others (2021). The role of diffuse electron precipitation in the formation of subauroral polarization streams. *Journal of Geophysical Research: Space Physics*, *126*(12), e2021JA029792. doi: 10.1029/2021JA029792

Liu, J., Hu, H., Han, D., Yang, H., & Lester, M. (2015). Simultaneous ground-based optical and superdarn observations of the shock aurora at mlt noon. *Earth, Planets and Space*, *67*(1), 1–18. doi: https://doi.org/10.1186/s40623-015-0291-2

Mannucci, A. J., Tsurutani, B. T., Iijima, B. A., Komjathy, A., Saito, A., Gonzalez, W. D., . . . Skoug, R. (2005). Dayside global ionospheric response to the major interplanetary events of october 29–30, 2003 "halloween storms". *Geophysical Research Letters*, *32*(12). Retrieved from `https://agupubs.onlinelibrary.wiley.com/doi/abs/10.1029/2004GL021467` doi: https://doi.org/10.1029/2004GL021467

Menk, F. W., Yeoman, T. K., Wright, D. M., Lester, M., & Honary, F. (2003). High-latitude observations of impulse-driven ULF pulsations in the ionosphere and on the ground. *Annales Geophysicae*, *21*(2), 559–576. Retrieved from `https://angeo.copernicus.org/articles/21/559/2003/` doi: 10.5194/angeo-21-559-2003

Merkin, V., & Lyon, J. (2010). Effects of the low-latitude ionospheric boundary condition on the global magnetosphere. *Journal of Geophysical Research: Space Physics*, *115*(A10). doi: 10.1029/2010JA015461

Milan, S. E., Grocott, A., de Larquier, S., Lester, M., Yeoman, T. K., Freeman, M. P., & Chisham, G. (2013). Traveling ionospheric disturbances in the weddell sea anomaly associated with geomagnetic activity. *Journal of Geophysical Research: Space Physics*, *118*(10), 6608-6617. Retrieved from `https://agupubs.onlinelibrary.wiley.com/doi/abs/10.1002/jgra.50566` doi: https://doi.org/10.1002/jgra.50566

Nishitani, N., Ruohoniemi, J. M., Lester, M., Baker, J., Koustov, A. V., Shepherd, S., . . . others (2019). Review of the Accomplishments of Mid-latitude Super Dual Auroral Radar Network (SuperDARN) HF Radars. *Progress in Earth and Planetary Science*.

Ozturk, D. S., Zou, S., Ridley, A. J., & Slavin, J. A. (2018). Modeling study of the geospace system response to the solar wind dynamic pressure enhancement on 17 march 2015. *Journal of Geophysical Research: Space Physics*, *123*(4), 2974-2989. Retrieved from https://agupubs.onlinelibrary.wiley.com/doi/abs/10.1002/2017JA025099 doi: https://doi.org/10.1002/2017JA025099

Pham, K., Zhang, B., Sorathia, K., Dang, T., Wang, W., Merkin, V., ... others (2022). Thermospheric density perturbations produced by traveling atmospheric disturbances during august 2005 storm. *Journal of Geophysical Research: Space Physics*, *127*(2), e2021JA030071. doi: 10.1029/2021JA030071

Ponomarenko, P. V., Menk, F. W., & Waters, C. L. (2003). Visualization of ULF waves in SuperDARN data. *Geophysical Research Letters*, *30*(18), 1926. Retrieved from https://agupubs.onlinelibrary.wiley.com/doi/abs/10.1029/2003GL017757 doi: https://doi.org/10.1029/2003GL017757

Richmond, A., Ridley, E., & Roble, R. (1992). A thermosphere/ionosphere general circulation model with coupled electrodynamics. *Geophysical Research Letters*, *19*(6), 601–604. doi: 10.1029/92GL00401

Shepherd, S. G. (2014). Altitude-adjusted corrected geomagnetic coordinates: Definition and functional approximations. *Journal of Geophysical Research: Space Physics*, *119*(9), 7501-7521. Retrieved from https://agupubs.onlinelibrary.wiley.com/doi/abs/10.1002/2014JA020264 doi: 10.1002/2014JA020264

Shi, X., Hartinger, M. D., Baker, J. B. H., Murphy, B. S., Bedrosian, P. A., Kelbert, A., & Rigler, E. J. (2022). Characteristics and sources of intense geoelectric fields in the united states: Comparative analysis of multiple geomagnetic storms. *Space Weather*, *n/a*(n/a), e2021SW002967. Retrieved from https://agupubs.onlinelibrary.wiley.com/doi/abs/10.1029/2021SW002967 doi: https://doi.org/10.1029/2021SW002967

Singer, H., Matheson, L., Grubb, R., Newman, A., & Bouwer, D. (1996). Monitoring space weather with the goes magnetometers. In *Goes-8 and beyond* (Vol. 2812, pp. 299–308). doi: 10.1117/12.254077

Sorathia, K., Merkin, V., Panov, E., Zhang, B., Lyon, J., Garretson, J., ... Wiltberger, M. (2020). Ballooning-interchange instability in the near-earth plasma sheet and auroral beads: Global magnetospheric modeling at the limit of the mhd approximation. *Geophysical research letters*, *47*(14), e2020GL088227. doi: 10.1029/2020GL088227

Toffoletto, F., Sazykin, S., Spiro, R., & Wolf, R. (2003). Inner magnetospheric modeling with the rice convection model. *Space Science Reviews*, *107*(1-2), 175–196. doi: 10.1023/A:1025532008047

Weygand, J. M. (2009a). *Equivalent Ionospheric Currents (EICs) derived using the Spherical Elementary Currents Systems (SECS) technique at 10 sec Resolution in Geographic Coordinates.* UCLA. doi: https://doi.org/10.21978/P8D62B

Weygand, J. M. (2009b). *Spherical Elementary Current (SEC) Amplitudes derived using the Spherical Elementary Currrent Systems (SECS) technique at 10 s Resolution in Geographic Coordinates.* UCLA. doi: https://doi.org/10.21978/P8PP8X

Weygand, J. M., Amm, O., Viljanen, A., Angelopoulos, V., Murr, D., Engebretson, M. J., ... Mann, I. (2011). Application and validation of the spherical elementary currents systems technique for deriving ionospheric equivalent currents with the north american and greenland ground magnetometer arrays. *Journal of Geophysical Research: Space Physics*, *116*(A3). Retrieved from https://agupubs.onlinelibrary.wiley.com/doi/abs/10.1029/2010JA016177 doi: https://doi.org/10.1029/2010JA016177

Yu, Y.-Q., & Ridley, A. J. (2011). Understanding the response of the ionosphere-magnetosphere system to sudden solar wind density increases. *Journal of Geophysical Research: Space Physics*, *116*(A4). Retrieved from https://agupubs.onlinelibrary.wiley.com/doi/abs/10.1029/2010JA015871 doi: https://

doi.org/10.1029/2010JA015871

Zhang, B., Sorathia, K. A., Lyon, J. G., Merkin, V. G., Garretson, J. S., & Wiltberger, M. (2019). Gamera: A three-dimensional finite-volume mhd solver for non-orthogonal curvilinear geometries. *The Astrophysical Journal Supplement Series*, *244*(1), 20. doi: 10.3847/1538-4365/ab3a4c

Zhang, R., Liu, L., Chen, Y., Le, H., & Zhang, H. (2022). Ulf fluctuation of low-latitude ionospheric electric fields during sudden commencements. *Journal of Geophysical Research: Space Physics*, *127*(3), e2021JA030012. Retrieved from `https://agupubs.onlinelibrary.wiley.com/doi/abs/10.1029/2021JA030012` (e2021JA030012 2021JA030012) doi: https://doi.org/10.1029/2021JA030012

Zhou, X., Haerendel, G., Moen, J. I., Trondsen, E., Clausen, L., Strangeway, R. J., ... Lorentzen, D. A. (2017). Shock aurora: Field-aligned discrete structures moving along the dawnside oval. *Journal of Geophysical Research: Space Physics*, *122*(3), 3145-3162. Retrieved from `https://agupubs.onlinelibrary.wiley.com/doi/abs/10.1002/2016JA022666` doi: https://doi.org/10.1002/2016JA022666

Zong, Q.-G., Zhou, X.-Z., Wang, Y. F., Li, X., Song, P., Baker, D. N., ... Pedersen, A. (2009). Energetic electron response to ulf waves induced by interplanetary shocks in the outer radiation belt. *Journal of Geophysical Research: Space Physics*, *114*(A10). Retrieved from `https://agupubs.onlinelibrary.wiley.com/doi/abs/10.1029/2009JA014393` doi: https://doi.org/10.1029/2009JA014393

Zou, S., Ozturk, D., Varney, R., & Reimer, A. (2017). Effects of sudden commencement on the ionosphere: PFISR observations and global MHD simulation. *Geophysical Research Letters*, *44*(7), 3047-3058. Retrieved from `https://agupubs.onlinelibrary.wiley.com/doi/abs/10.1002/2017GL072678` doi: https://doi.org/10.1002/2017GL072678